

Predictive Modeling of Transient Storage and Nutrient Uptake: Implications for Stream Restoration

Ben L. O'Connor¹; Miki Hondzo²; and Judson W. Harvey³

Abstract: This study examined two key aspects of reactive transport modeling for stream restoration purposes: the accuracy of the nutrient spiraling and transient storage models for quantifying reach-scale nutrient uptake, and the ability to quantify transport parameters using measurements and scaling techniques in order to improve upon traditional conservative tracer fitting methods. Nitrate (NO₃⁻) uptake rates inferred using the nutrient spiraling model underestimated the total NO₃⁻ mass loss by 82%, which was attributed to the exclusion of dispersion and transient storage. The transient storage model was more accurate with respect to the NO₃⁻ mass loss ($\pm 20\%$) and also demonstrated that uptake in the main channel was more significant than in storage zones. Conservative tracer fitting was unable to produce transport parameter estimates for a riffle-pool transition of the study reach, while forward modeling of solute transport using measured/scaled transport parameters matched conservative tracer breakthrough curves for all reaches. Additionally, solute exchange between the main channel and embayment surface storage zones was quantified using first-order theory. These results demonstrate that it is vital to account for transient storage in quantifying nutrient uptake, and the continued development of measurement/scaling techniques is needed for reactive transport modeling of streams with complex hydraulic and geomorphic conditions.

DOI: 10.1061/(ASCE)HY.1943-7900.0000180

CE Database subject headings: Restoration; Nutrient loads; Transport phenomena; Fluvial hydraulics; Surface waters.

Author keywords: Restoration; Nutrient loads; Transport phenomena; Fluvial Hydraulics; Surface waters.

Introduction

Understanding how geomorphology and hydraulics influence nutrient uptake is vital for stream restoration projects that modify the channel in order to improve water quality. There is empirical evidence that nutrient uptake rates are enhanced in natural and constructed geomorphic features such as in-channel and backwater pools (Ensign and Doyle 2005; Opdyke et al. 2006; Bukaveckas 2007), debris dams of leaf litter and coarse woody material (Bernhardt et al. 2003; Groffman et al. 2005; Roberts et al. 2007), dense algal mats (Kim et al. 1992; Gooseff et al. 2004), and in the hyporheic flowpaths (Holmes et al. 1996; Kasahara and Hill 2006), which contain complex hydraulic conditions generating longer residence times (transient storage). However, quantifying and predicting the degree of nutrient uptake in relation to stream characteristics is challenging. Many restoration projects involving channel reconfiguration and in-stream habitat modification have attempted to mimic these natural features in order to generate

greater connectivity between the channel and its biogeochemically active sediments, surface storage zones, and riparian environments (Craig et al. 2008). Unfortunately, there has been very little documented evidence of the effectiveness of such restoration projects (Bernhardt et al. 2005). This lack of data hinders the development of predictive reactive transport models for restoration, but there are also limitations in the current methodologies for quantifying nutrient uptake rates and transport processes individually that need to be addressed as well.

Nutrient and isotope additions (reactive tracers) characterize the majority of studies providing information on reach-scale nutrient uptake rates (e.g., Mulholland et al. 2008). Virtually all of these studies have used the nutrient spiraling model (Newbold et al. 1981), which is a simplification of the one-dimensional (1D) advection-dispersion equation and assumes advective transport only. Conversely, researchers examining transport in streams have focused on transient storage processes that include groundwater and hyporheic exchange (e.g., Harvey and Wagner 2000), as well as mixing with surface storage zones in the channel (e.g., Gooseff et al. 2005). Many of these type of studies have been used to develop and refine the transient storage model, which adds terms (and in some cases additional equations) to the 1D advection-dispersion equation to account for transient storage processes. A disproportionately small number of studies have applied transient storage processes in the interpretation of nutrient uptake rates (Triska et al. 1989; Gooseff et al. 2004), and only recently has there been work comparing and contrasting nutrient uptake rates using the nutrient spiraling and transient storage models (Runkel 2007).

Previous studies examining reach-scale nutrient uptake rates in relation to geomorphology and hydrology have been done using intersite comparisons. This approach is limited in its ability to quantify physical-biogeochemical interactions because within-

¹Environmental Engineer, Environmental Sciences Div., Argonne National Laboratory, EVS-240, Argonne, IL 60439; formerly, NRC Postdoctoral Associate, U.S. Geological Survey, Reston, VA (corresponding author). E-mail: boconnor@anl.gov

²Professor, Dept. of Civil Engineering, St. Anthony Falls Laboratory, Univ. of Minnesota-Twin Cities, 2 Third Ave. SE, Minneapolis, MN 55414.

³Hydrologist, U.S. Geological Survey, Mail Stop 430 National Center, Reston, VA 20192.

Note. This manuscript was submitted on February 24, 2009; approved on October 9, 2009; published online on November 9, 2009. Discussion period open until May 1, 2011; separate discussions must be submitted for individual papers. This paper is part of the *Journal of Hydraulic Engineering*, Vol. 136, No. 12, December 1, 2010. ©ASCE, ISSN 0733-9429/2010/12-1018-1032/\$25.00.

reach variability in stream characteristics are integrated (Orr et al. 2009), and that the nutrient uptake metrics of the nutrient spiraling model are not independent of the system's hydraulic and geomorphic conditions (Runkel 2007). It is desirable to couple predictions of transport processes and nutrient uptake rates in terms of geomorphic variables because channel form and hydraulic conditions are the engineering parameters used in stream restoration designs (Shields et al. 2003). Unfortunately, the relationship between biological communities and biogeochemical processes with geomorphic and hydraulic conditions is not fully realized and the most likely means to develop predictive models of nutrient uptake is through regression and scaling approaches using reach-scale nutrient uptake measurements. This approach is analogous to regional-scale nutrient models that relate uptake kinetics to watershed characteristics (e.g., Alexander et al. 2009), as well as microcosm nutrient uptake measurements that have sought to address spatial variability in uptake results based on the local sediment type, organic content, and flow conditions (Kemp and Dodds 2002; Richardson et al. 2004; Smith et al. 2006; O'Connor et al. 2006).

The development of regression and scaling models relating nutrient uptake to geomorphic and hydraulic variables requires the synthesis of accurately measured nutrient uptake rates and the ability to relate them to specific physical conditions of the stream. One confounding issue with this approach is that biogeochemical mechanisms for nutrient uptake are biologically mediated, which requires knowledge about the interactions between physical processes with the abundance and location of biological communities (e.g., Warnars et al. 2007). The assumption that transient storage exerts primary control over biogeochemical reaction rates is often made (implying that biological communities are most active in hyporheic and surface storage zones), but empirical evidence from several studies is equivocal on this issue (Ensign and Doyle 2006). Another obstacle is the difficulty in measuring nutrient uptake kinetics. This often involves many biogeochemical reaction pathways, which are analytically difficult to isolate, often expensive, and time consuming to obtain, and the measurement techniques need to be applied over a defined sample volume, typically a microcosm (patch scale) or a reach (Groffman et al. 2006). The sample volume issue is critical to the development of predictive models of nutrient uptake. Reach-scale measurements of nutrient uptake (typically done with a stream tracer experiment) are desirable for restoration purposes as they directly apply to the downstream conveyance of nutrient loads and are on the same order as typical stream restoration projects in terms of the spatial scale examined. A complicating factor to reach-scale nutrient uptake measurements is that they are inherently linked to a transport model, so the accuracy of the nutrient uptake rate measurement is dependent upon the ability to quantify transport processes.

Because the development of predictive reactive transport models for stream restoration requires synthesis of empirical data, a crucial first step is to ensure that transport processes are accurately represented in the quantification of reach-scale nutrient uptake rates. The focus of this study was to examine the two most commonly used reactive transport models for inferring nutrient uptake: the nutrient spiraling and transient storage models. A stream tracer experiment was combined with hydraulic and channel form measurements in order to: (1) assess the effects of transient storage and dispersion on NO_3^- uptake rates and (2) evaluate the ability to predict transient storage parameters based on physical measurements and scaling relationships. The study was conducted on Elder Creek, a relatively undisturbed, forested wa-

tershed which typically has low NO_3^- concentrations ($<50 \mu\text{g/L}$ as N). This site has characteristics that are comparable to what a restoration project may encounter such as a confined valley, limited hyporheic zone (shallow bedrock in this case rather than silted-in or armored sediments), and flashy hydrology, as well as features that are often desirable in final restoration designs, such as pool-riffle sequences, large boulders along banks and in the channel, a stable bed, and surface storage zones with large recirculating eddies.

Background Information

1D Reactive Transport Models

Reach-scale nutrient uptake measurements are dependent upon using a reactive transport model. Typically, the starting point is the 1D advection-dispersion equation

$$\frac{\partial C}{\partial t} + \frac{Q}{A} \frac{\partial C}{\partial x} = \frac{1}{A} \left(A D_x \frac{\partial C}{\partial x} \right) - \lambda C \quad (1)$$

where C =solute concentration; t =time; Q =stream discharge; A =cross-sectional area; x =distance downstream; λ =first-order uptake rate coefficient; and D_x =longitudinal dispersion coefficient (groundwater discharge is not considered). The nutrient spiraling model (Newbold et al. 1981) assumes that nutrient concentrations are at steady state, Q and A do not vary over the reach, and that transport is controlled by advection only, so Eq. (1) simplifies to

$$U \frac{dC}{dx} = -\lambda C \quad (2)$$

where U =cross-sectionally averaged velocity (assumed constant over the entire reach). Integrating Eq. (2) and introducing the nutrient spiraling uptake length ($S_w = U/\lambda$) gives an expression for C as a function of the downstream distance

$$C = C_o e^{-(x/S_w)} \quad (3)$$

where C_o =solute concentration at the beginning of the reach. Nutrient concentration data are collected along the stream reach (ambient or during the tracer plateau) and plotted on a semilogarithmic scale versus distance downstream, which produces a linear trend according to Eq. (3) where the slope is the inverse of S_w .

The most widely used version of the transient storage model adds an additional term to Eq. (1) representing exchange with storage zones (both surface and hyporheic), as well as an additional equation to track concentrations within the storage zones resulting in

$$\frac{\partial C}{\partial t} + \frac{Q}{A} \frac{\partial C}{\partial x} = \frac{1}{A} \left(A D_x \frac{\partial C}{\partial x} \right) + \alpha (C_s - C) - \lambda C \quad (4)$$

$$\frac{dC_s}{dt} = \alpha \frac{A}{A_s} (C - C_s) - \lambda_s C_s \quad (5)$$

where α =storage zone exchange coefficient; C_s =solute concentration in the storage zone; A_s =cross-sectional area of the storage zone; λ =first-order reaction coefficient in the channel; and λ_s =first-order reaction coefficient in the storage zone. Runkel (1998) developed the 1D transport with inflow and storage (OTIS) model that uses a Crank-Nicolson finite difference method for solving Eqs. (4) and (5).

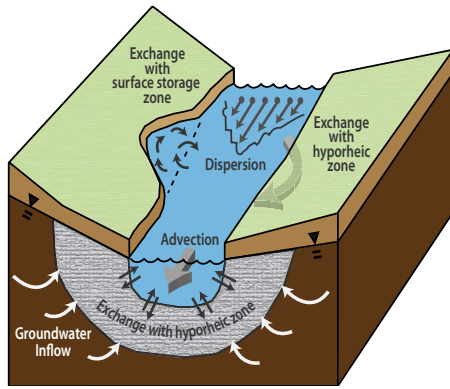


Fig. 1. Schematic of transport processes relating to transient storage in streams

Quantifying Transport Parameters

The interaction of hydraulics and channel form generates a variety of transport processes associated with transient storage in rivers and streams (Fig. 1). The 1D reactive transport models described by Eqs. (1)–(5) contain the transport parameters Q , U , D_x , A , A_s , and α that can be measured or estimated using a variety of techniques.

Stream Tracer Experiment

One of the most common ways to quantify reactive transport is through the analysis of a stream tracer experiment, which involves the coinjection of a conservative and a reactive tracer. Quantifying transport parameters is done by inverse modeling of the conservative tracer concentration breakthrough curves at fixed points along the stream. This approach has the advantage that the fitted transport parameters are reach-averaged values so they account for two-dimensional (2D) and three-dimensional (3D) complexities in transport processes. However, the resulting transport parameter estimates are specific to the hydraulic and channel conditions at the time of the tracer experiment, which limits their use of predictive modeling for different channels or flow conditions.

Physical Measurements

Cross-sectional profiles of depth and velocity can give values of Q , U , and A using traditional surveying and stream gauging techniques. However, measurements of D_x , A_s , and α are more challenging given the 3D nature of open channel flows and that transient storage is generated by both hyporheic and surface exchange zones. In this section we describe how D_x can be quantified using velocity profiles and how A_s and α can be quantified for surface storage zones.

The longitudinal dispersion coefficient (D_x) is essentially a cross-sectional average of advection, molecular diffusion, and turbulence processes that produce vertical and transverse variation in velocities. Fischer (1967) showed that transverse mixing was more important than vertical mixing in determining D_x based on shear dispersion theory, and that D_x can be estimated using cross-sectional velocity contours according to

$$D_x = -\frac{1}{A} \int_0^B (\bar{u} - U) h dy \int_0^y \frac{1}{D_y h} dy' \int_0^{y'} (\bar{u} - U) h dy'' \quad (6)$$

where B =stream width; y =transverse coordinate; h =local water depth; \bar{u} =depth-averaged velocity; and D_y =transverse mixing co-

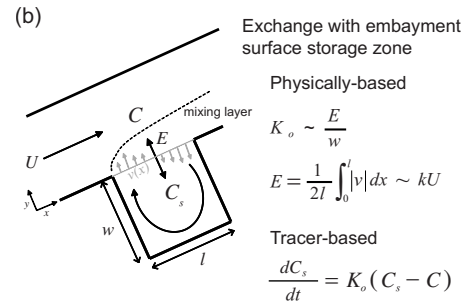


Fig. 2. Solute exchange with surface transient storage zone: (a) photograph of the embayment storage zone located at $x=60$ m; (b) diagram of exchange processes between the main channel and the embayment storage zone

efficient [estimated as $D_y=0.6u_*h$, where u_* =shear stress velocity (Rutherford 1994)].

Exchange with embayment surface storage zones is the result of the sudden expansion of the channel cross section generating a mixing layer between the embayment and the downstream flow (Fig. 2). The exchange of water between the main channel and the embayment is facilitated by the transverse velocity gradients within the mixing layer and the shedding of large, 2D coherent structures forming characteristic gyre formations dependent upon the geometry of the embayment (Uijttewaal et al. 2001). Solute exchange is quantified as a first-order process related to the geometry between main channel and the storage zone (Valentine and Wood 1979; Uijttewaal et al. 2001). Assuming the surface storage zone can be characterized by a length (l), width (w), and depth (h_s) and that the exchange is driven by a nondirectional entrainment velocity [E , Fig. 2(b)] then the change in solute concentration within the storage zone follows:

$$\frac{dC_s}{dt} = -\frac{E}{w h_s} (C_s - C) \quad (7)$$

where h =depth at the channel-storage zone interface (typically the depth in the channel is assumed). Several flume experiments have used conservative tracers and Eq. (7) to measure E over a wide range in embayment geometries, which have been used to suggest that

$$E = kU \quad (8)$$

where k =dimensionless exchange coefficient ranging from 0.01 $< k < 0.03$ (Valentine and Wood 1979; Uijttewaal et al. 2001) and 0.01 $< k < 0.05$ (Weitbrecht et al. 2008) and U =average velocity in the main channel. Quantifying solute exchange between the main channel and the surface storage zone in this fashion implies that the exchange process can be described solely by a first-order exchange coefficient ($K_o=Eh/wh_s$), which can be done using

physical- or tracer-based approaches. Quantifying E according to Eq. (8) results in

$$K_o = \frac{kU h}{w h_s} \quad (9)$$

which can be related to the reach-averaged exchange coefficient (α) according to

$$\alpha = K_o \frac{A_s}{A} \quad (10)$$

where A_s =interfacial area between the surface storage zone and the main channel.

Empirical Scaling Relationships

A variety of empirical scaling relationships have been developed that relate transport parameters (quantified using stream tracer experiments) to measurable hydraulic and channel form values under a variety of stream conditions. Scaling approaches have been used primarily to quantify D_x in streams with varying hydraulic and geomorphic characteristics (see Seo and Cheong 1998, for a review of various methods). One example is the expression proposed by Fischer (1975) that estimates the triple integration of Eq. (6) as

$$D_x = 0.011 \frac{U^2 B^2}{u_* h} \quad (11)$$

Less attention has been given to the transient storage terms A_s and α . Stream tracer data from relatively straight channels in the Tennessee Valley region (Thackston and Schnelle 1970) and from more than 50 streams across the United States (Harvey and Wagner 2000) have been used to scale A_s to channel roughness. An expression for A_s was derived by fitting a power law to the data presented in Fig. 12 of Harvey and Wagner (2000) resulting in

$$\frac{A_s}{A} = 0.097 f^{0.42} \quad (12)$$

where f =Darcy-Weisbach friction factor and the scaling equation had an $R^2=0.72$. Cheong et al. (2007) used dimensional analysis with stream tracer data from 35 streams in the United States to derive scaling expressions for transient storage transport parameters based on hydraulic and channel characteristics. Their expression for α resulted in

$$\frac{\alpha}{h/u_*} = 20.595 \left(\frac{A_s}{A} \right) \left(\frac{U}{u_*} \right)^{-1.463} \left(\frac{B}{h} \right)^{0.664} \left(\frac{UL}{D_x} \right)^{0.323} Si^{1.913} \quad (13)$$

where Si =reach sinuosity ratio and the regression parameters had a correlation coefficient of 0.81 using the robust minimum covariance determinant method. To the best of our knowledge, this is the only available predictive expression for α currently available.

Methods

Study Site

Elder Creek is a second order tributary of the South Fork Eel River located in the Angelo Coast Range Reserve (ACRR), Mendocino County, northern California with a drainage area of 17 km². The study reach is located downstream of USGS streamflow-gauging station 11475560 (39°43'47"N, 123°38'34"W). This investigation was performed in late July 2005 with a reach-steady discharge (Q) of 0.205 m³/s. The

Table 1. Average Channel Geometry and Velocity Characteristics of the Upper, Middle, and Lower Physical Reaches

Parameter	Upper pool	Middle riffle	Lower pool
x (m)	0–30	30–70	70–100
B (m)	5.37	5.03	5.23
h (m)	0.27	0.11	0.19
A (m ²)	1.97	0.57	1.06
U (m/s)	0.10	0.36	0.19
u_* (m/s)	0.02	0.10	0.03

100-m study reach had a slope of 0.026, sinuosity ratio (Si) of 1.1, limited hyporheic zone, and contained three subreaches with distinct differences in channel form and hydraulic conditions [Table 1 and Figs. 3(a and b)]. A narrow high gradient riffle was used as a mixing zone for the solute tracer injection and defines the upstream extent of the study reach. Below this riffle, the upper reach is a 30-m long pool with a fairly uniform cross section [Fig. 3(c)]. The middle reach is a 40-m long riffle with boulder obstructions throughout [Fig. 3(d)]. The boulders create a complex flow field with small recirculation eddies behind individual boulders up to large-scale embayments with recirculation zones on the order of 1 m² in surface area. A large embayment, 1.5 m in length by 1.0 m wide (Fig. 2), was located near the end of the middle reach ($x=60$ m) that was used to assess exchange with surface storage zones. The lower reach is a shallow pool, 40 m in length [Fig. 3(e)]. The center of the channel in this reach contains bed-rock outcroppings that diverts the flow to the banks, generating recirculating eddies.

Field Measurements and Stream Tracer Experiment

Stream width and water depth measurements were made at transects every 10 m along the study reach. The streamwise (u) and transverse (v) velocity components were measured using a Flow-Tracker (SonTek, San Diego) acoustic-Doppler velocimeter (ADV) and a StreamPro (Teledyne RD Instruments, San Diego) acoustic-Doppler current profiler (ADCP). ADV profiles were measured across several transects, as well as at point locations with shallow flow depths (<20 cm). The ADCP scans of velocity and bed topography were limited to the pool regions of the upper and lower reaches and were performed by traversing the probe across the stream at a speed of approximately 1 cm/s. This resulted in velocity data being collected at 0.02-m depth segments approximately every 0.1 m across the transect. Velocity contour maps were generated by interpolating the measured velocities (irregular grid) to a regular grid of 0.3 m horizontal by 0.03 m vertical using triangular-based linear interpolation.

The stream tracer experiment consisted of a 75-min constant-rate injection (75 mL/min) of a sodium chloride (conservative tracer) and potassium nitrate (reactive tracer) solution. The experiment targeted a 10-fold increase in chloride (Cl^-) and NO_3^- above ambient concentrations (approximately 1.5 mg/L and 20 μ g/L as N, respectively) in order to guarantee measurement detection levels. A 10-fold increase in NO_3^- concentration is larger than what has been used typically for nutrient uptake experiments. However, the intention of the NO_3^- addition was to assess how physical factors of the stream reach affected uptake rates, so it was desirable to force a substantial uptake response by elevating the NO_3^- concentrations well above ambient levels (uptake limiting). Specific conductivity was used as a surrogate for Cl^- concentrations and was measured at 1 min intervals at locations

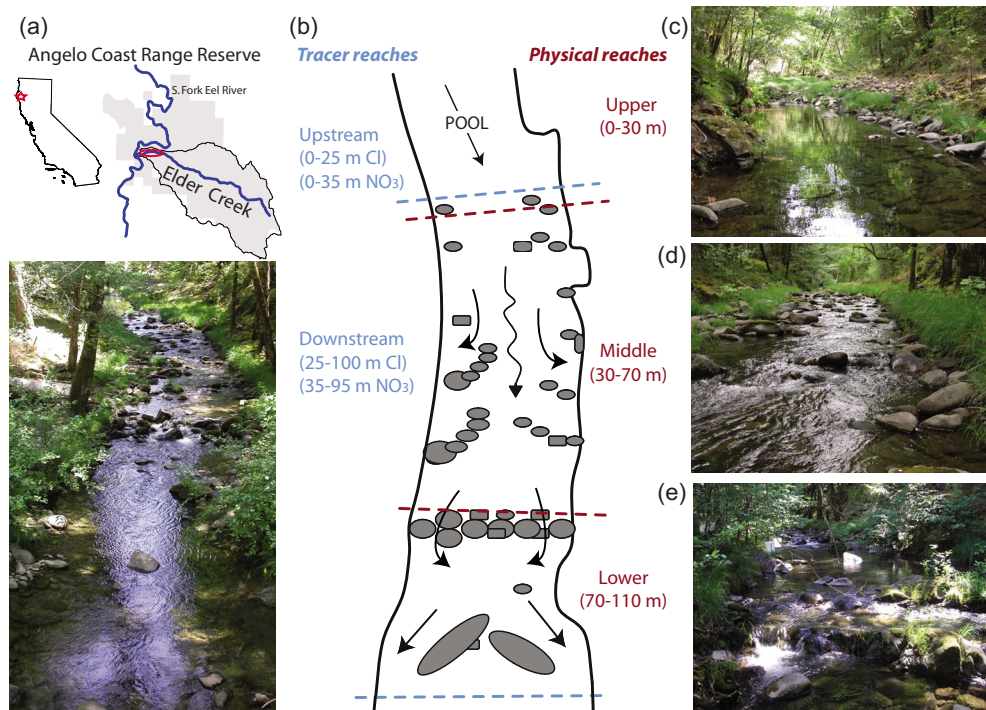


Fig. 3. Elder Creek study reach: (a) location of the Angelo Coast Range Reserve and a photo of the reach; (b) diagram of the reach showing the physical differences among the upper, middle, and lower reaches, as well as showing the upstream and downstream tracer reaches; (c) photo of the upper reach; (d) photo of the middle reach; and (e) photo of the lower reach

located at 25, 60, and 100 m downstream of the injection site that closely match the endpoints of the upper, middle, and lower reaches [Fig. 3(b)]. The specific conductivity also was measured in the embayment surface storage zone located 60 m downstream of the injection site (Fig. 2). Water grab samples were collected during the plateau of the tracer injection experiment (when specific conductivity reached a maximum and steady value). Biosensors recorded NO_3^- concentrations at 1-min intervals and were located at 35 and 95 m downstream of the injection site representing locations near the end of the upper and lower reaches [Fig. 3(b)].

Specific conductivity was measured using a Hydrolab (Hach Company, Loveland, Colorado) Data-sonde 4a. NO_3^- concentrations were measured analytically from grab samples and in situ using biosensor technology. Grab samples were filtered using 0.45- μm membrane syringe filters and stored at 4°C until analyzed. NO_3^- and nitrite (NO_2^-) concentrations were determined using the Cd-reduction method (4500 NO_3^- -F [American Public Health Association (APHA) 1998]) on a Lachat QuickChem 8000 flow injection autoanalyzer (Hach Company, Loveland, Colorado). Time series data of NO_3^- concentrations were measured using NO_3^- biosensors (Unisense A/S, Aarhus, Denmark), which use an ion permeable membrane with a bacterial chamber containing microbes conditioned for denitrification with nitrous oxide (N_2O) end product. The signal from the N_2O transducer of the biosensors was channeled to a PA2000 picoammeter (Unisense) for signal amplification.

Inverse modeling was used to determine the reactive transport parameters for the transient storage model described by Eqs. (4) and (5). The OTIS-P model (OTIS with parameter estimation by nonlinear regression) used the specific conductivity time series data to solve for the transport parameters D_x , A , A_s , and α (Q was measured from velocity and transect data). These transport pa-

rameters were used along with NO_3^- concentrations measured by the biosensors to quantify the reaction terms λ and λ_x using the OTIS-P model. Logistical issues did not allow for the specific conductivity and biosensor NO_3^- measurements to be taken at the same locations, so the upstream and downstream reaches of the conservative (Cl^-) and reactive (NO_3^-) tracer experiments varied slightly. The upstream tracer reach was from 0–25 m for Cl^- and 0–35 m for NO_3^- , while the downstream tracer reach was from 25–100 m for Cl^- and from 35–95 m for NO_3^- [Fig. 3(b)]. For the nutrient spiraling model, the NO_3^- concentration grab samples collected during the tracer plateau along the reach were used to determine S_w according to Eq. (3).

Comparison of Measured/Scaled and Tracer-Fitted Transport Parameters

Measured and scaled values of the transport parameters (D_x , A , A_s , and α) were used to simulate conservative tracer breakthrough curves using OTIS for comparison with the conservative stream tracer fits of the values using OTIS-P. The goodness of fit between simulated and tracer breakthrough curves was evaluated as RMS-error values (RMSE). For the forward modeling of transport parameters using measured and scaled values, direct measurements were preferred to scaled values. Cross-sectional transect data collected every 10 m was averaged over the upper, middle, and lower physical reaches to obtain values for A . Estimates of D_x based on ADCP measurements [Eq. (6)] were used for the upper and lower physical reaches and D_x was evaluated according to Eq. (11) for the middle-riffle reach where transverse velocity profiles were not obtainable. The large embayment surface storage zone in the middle reach ($x=60$ m) was assumed to control the transient storage of that reach so measured values of A_s (interfacial area) and α [Eq. (10)] were used. For the upper and lower physical

reaches, the scaling relationships for A_s [Eq. (12)] and α [Eq. (13)] were used because direct measurements were not possible in these pool reaches where transient storage was assumed to occur in dead zones of undefined geometry.

Evaluation of Transient Storage and Nutrient Uptake Parameters

The effects of transient storage on nutrient uptake were evaluated using a variety of metrics developed by Runkel (2002, 2007) for quantifying residence times and uptake partitioning between the main channel and storage zones. The mean travel time in the main channel (t_c) and in the storage zone (t_s), as well as the fraction of the mean travel time due to transient storage (F_{med}) were evaluated according to

$$t_c = \frac{LU + 2D}{U^2} \quad (14)$$

$$t_s = \frac{A_s}{A} \left(\frac{LU + 2D}{U^2} \right) \quad (15)$$

$$F_{\text{med}} = \frac{A_s}{A + A_s} (1 - e^{-L(\alpha/U)}) \quad (16)$$

The relative uptake between the main channel and the storage zone was estimated by calculating the change in mass of NO_3^- (area under the tracer curve, $M = \int QC dt$) between simulations assuming transport only (M_t), reactive transport (M_r), uptake only in the main channel (M_c), and uptake only in the storage zone (M_s) simulations. The total mass loss (ΔM) was calculated assuming reactive transport ($\Delta M_{\text{total}} = M_r - M_r$), reaction in the main channel only ($\Delta M_{\text{channel}} = M_r - M_c$), and reaction in the storage zone only ($\Delta M_{\text{storage}} = M_r - M_s$). Finally, the percent uptake occurring in the main channel and the storage zone were estimated as

$$\text{Uptake in channel (\%)} = \frac{\gamma \Delta M_{\text{channel}}}{\Delta M_{\text{total}}} \times 100 \quad (17)$$

$$\text{Uptake in storage (\%)} = \frac{\gamma \Delta M_{\text{storage}}}{\Delta M_{\text{total}}} \times 100 \quad (18)$$

where $\gamma = \Delta M_{\text{total}} / (\Delta M_{\text{channel}} + \Delta M_{\text{storage}})$ is a correction factor accounting for the fact that simulations for channel and storage zone uptake slightly overestimate the total uptake (Runkel 2007).

In a similar fashion, a comparison of NO_3^- uptake rates between the nutrient spiraling and transient storage models was performed by calculating the change in NO_3^- mass (integration of breakthrough curves) over a reach, with the biosensor-measured NO_3^- breakthrough curves serving as the reference. The simulated NO_3^- breakthrough curves for the transient storage model were used to calculate the NO_3^- mass loss. For the nutrient spiraling model, the change in NO_3^- concentration over a reach was calculated using Eq. (3) and the NO_3^- mass loss as

$$\Delta M_{\text{spiraling}} = QC_o \frac{L}{U} (1 - e^{-L/S_w}) \quad (19)$$

which assumes that advection is the only transport process.

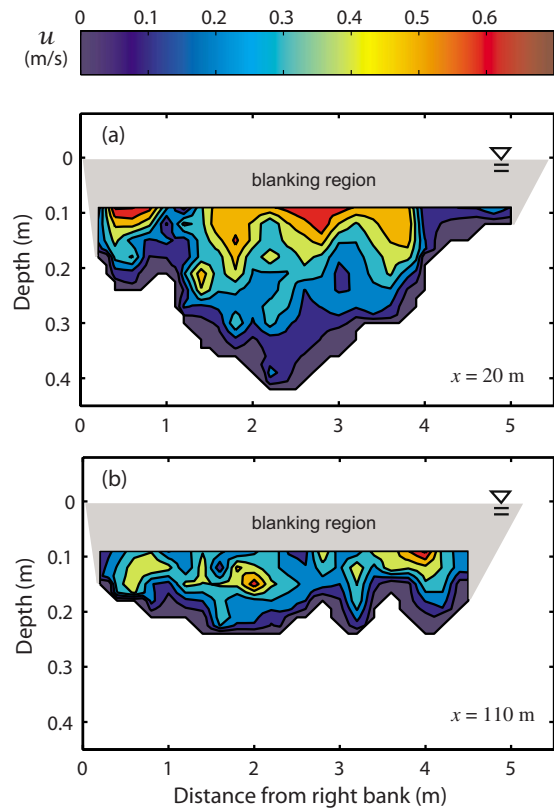


Fig. 4. Streamwise velocity (u) contour maps interpolated from ADCP measurements taken in (a) the upper reach; (b) the lower reach

Results

Physical Measurements and Scaling Estimates of Transport Parameters

Velocity contours from ADCP data for transects in the upper and lower physical reaches are shown in Figs. 4(a and b), respectively. The velocity contour map in the upper reach ($x=20$ m) demonstrated a clearly defined thalweg with higher velocities in the center of the channel and decreasing velocities with depth. On the contrary, the velocity contour map in the lower reach ($x=110$ m) did not demonstrate a defined thalweg, with more uniform velocities across the transect and with depth.

Estimates of D_x were obtained by evaluating ADCP velocity contours using Eq. (6) in a similar fashion to that described by Carr and Rehmann (2007) where velocities in the surface blanking region were estimated using both a constant and a linear fit of several near-surface velocities, while velocities in the bank region were ignored. The upper reach profile resulted in $D_x = 0.74$ m^2/s and the lower reach profile resulted in $D_x = 0.17$ m^2/s . An estimate of D_x using velocity profiles was not feasible in the middle-riffle reach because of its shallow water depths, and empirical scaling expression for D_x proposed by Fischer (1975) [Eq. (11)] resulted in $D_x = 2.00$ m^2/s . The estimate of A_s based on f [Eq. (12)] resulted in $A_s = 0.85$ m^2 , 0.07 m^2 , and 0.27 m^2 for the upper, middle, and lower physical reaches, respectively. The estimates of α [Eq. (13)] based on channel roughness (U/u_*), as well as channel form (B/h and Si) and the ratio of advective to dispersive mass transfer (UL/D_x) resulted in $\alpha = 4.09 \times 10^{-4}$ s^{-1} , 1.17×10^{-3} s^{-1} , and 2.73×10^{-4} s^{-1} for the upper, middle, and lower physical reaches, respectively.

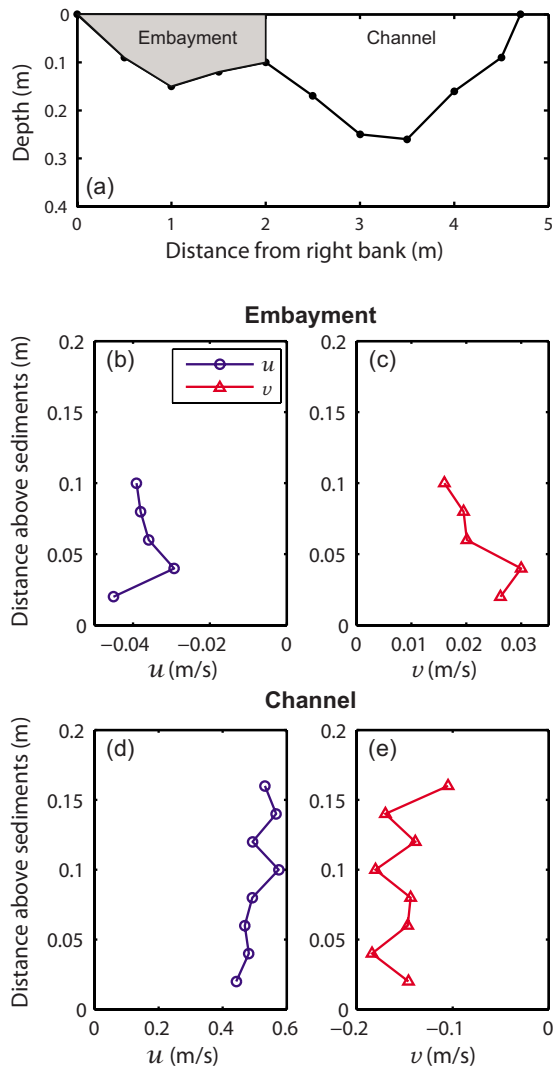


Fig. 5. ADV profiles at a transect located 60 m downstream with a naturally created embayment surface storage zone. (a) Water depth profile of the cross section, along with profiles of the streamwise (u) and transverse (v) velocity components within [(b) and (c)] the embayment and [(d) and (e)] the main channel, respectively

ADV velocity profiles at the large embayment surface storage zone of the middle reach ($x=60$ m) are shown in Figs. 5(b–e) for locations within the embayment and the adjacent main channel. The velocity profile near the center of the embayment depicted recirculating flow of a large coherent structure with negative u values (reverse flow) and v values directed toward the main channel [Figs. 5(b and c)]. The largest u and v values in the embayment were located near the sediments indicating a vorticity-driven momentum flux toward the sediments resulting from the large recirculation patterns. The velocity in the main channel was on the order of 50 cm/s with a substantial v component directed toward the embayment on the order of 15 cm/s [Figs. 5(d and e)]. A_s was estimated as the interfacial area between the embayment and the storage zone (0.23 m²), which was used with the geometry of the embayment and the average velocity in the main channel to estimate α according to Eqs. (9) and (10) resulting in $\alpha = 9.38 \times 10^{-3} \text{ s}^{-1}$.

Comparison of Forward and Inverse Transport Modeling

The OTIS-P fitted transport parameters (inverse model), as well as the measured and scaled transport parameters used for the forward model of specific conductivity breakthrough curves are listed in Table 2. Note that the downstream reach for the tracer experiment includes both the middle-riffle and lower-pool physical reaches. An attempt was made to fit transport parameters for both the middle and lower reaches separately, but the OTIS-P model was not able to produce a converged solution of transport parameters for each reach. The sharp transition between the middle-riffle and lower-pool reaches is shown by the difference in experimental Damkohler numbers (DaI) listed in Table 2. Most of the values are on the order of 0.1–1 (minimum uncertainty in estimates of transport parameters) except for the middle-riffle reach.

The transport parameters for the upstream tracer reach closely match the measured and scaled values for the upper physical reach. The transport parameters for the downstream tracer reach closely matched the measured and scaled values of the lower physical reach suggesting that the specific conductivity breakthrough curve was most sensitive to the transport-limiting mechanisms occurring within the lower reach pool. The coefficient of variation (COV) values for the inversely modeled transport parameters were relatively consistent and reasonable (Harvey and Wagner 2000), with exception to the estimates of A_s and α for the

Table 2. Estimates of the transport parameters (D_x , A , A_s , and α) and transient storage metrics (DaI , t_c , t_s , and F_{med}); results are given for transient storage model simulations using tracer-fitted (inverse model) and measured/scaled (forward model) transport parameters; values in brackets for the tracer-fitted model are the coefficients of variation for the parameter estimates

Reach	L (m)	D_x (m ² /s)	A (m ²)	A_s (m ²)	α (s ⁻¹)	DaI	t_c (min)	t_s (min)	F_{med}
Tracer-fitted transport parameters									
Upstream	25	0.68 [0.12]	2.13 [0.11]	0.92 [0.11]	5.69×10^{-4} [0.28]	0.5	6.8	2.9	0.04
Downstream	75	0.21 [0.44]	1.20 [0.06]	0.10 [1.37]	2.56×10^{-4} [2.72]	1.5	7.6	0.6	0.01
Measured and scaled transport parameters (scaled values noted)									
Upper	30	0.74	1.97	0.85 ^a	4.09×10^{-4} ^b	0.4	7.1	3.1	0.03
Middle	40	2.00 ^c	0.57	0.23	9.38×10^{-3}	4.0	2.4	0.9	0.19
Lower	30	0.17	1.06	0.27 ^a	2.73×10^{-4} ^b	0.2	2.7	0.7	0.01

^aScaled value using Eq. (12).

^bScaled value using Eq. (13).

^cScaled value using Eq. (11).

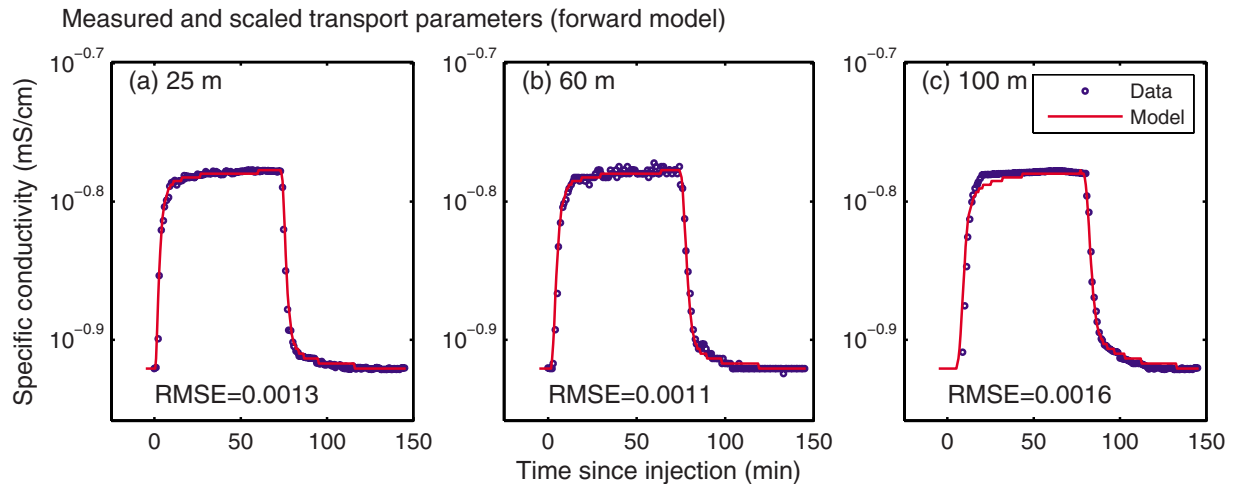


Fig. 6. Specific conductivity breakthrough curves located at (a) $x=25$ m; (b) $x=60$ m; and (c) $x=100$ m representing the upper, middle, and lower reaches, respectively. Simulated breakthrough curves were generated using transport parameters obtained using physical measurements and scaling relationships (forward model).

downstream tracer reach ($COV > 1$). The large uncertainty in estimating the transient storage parameters in the downstream reach was a result of the complex flow and channel morphology conditions over the riffle-pool transition, as mentioned previously.

The forward model simulations using measured and scaled transport parameters matched the specific conductivity breakthrough curves for the upper and middle reaches [Figs. 6(a and b)], as well as the tail of the lower reach but slightly underestimated the measured values for the rising limb of the tracer breakthrough curve [Fig. 6(c)]. The measured and simulated specific conductivity breakthrough curves using tracer-fitted transport parameters is shown in Fig. 7 (please note that the simulation at $x=60$ m [Fig. 7(b)] was not used to fit the transport parameters). The simulated breakthrough curves matched the measured specific conductivity values for the upstream and downstream reaches [Figs. 7(a and c)], but did not capture the onset of tracer decay and part of the tracer tail for the breakthrough curve located at $x=60$ m [Fig. 7(b)]. The RMSE values were similar between forward and inverse models except for the middle-riffle reach (x

$=60$ m) where the measured/scaled transport parameters did a better job of matching the measured specific conductivity values.

The transient storage metrics (t_c , t_s , and F_{med}) provided a greater contrast between the forward and inverse transport models (Table 2). The upstream inverse model and the upper forward model had similar transport parameters as they cover essentially the same reach. The inverse transport model for the downstream reach indicated there was little residence time within the storage zones. However, the forward model suggested a greater interaction with the storage zone, particularly in the middle-riffle reach which contained the largest F_{med} value.

Exchange with Surface Storage Zones

Solute exchange with the embayment surface storage zone ($x=60$ m) is shown by the difference in exponential decay between the relative specific conductivity values (Ω_c and Ω_s , baseline sub-

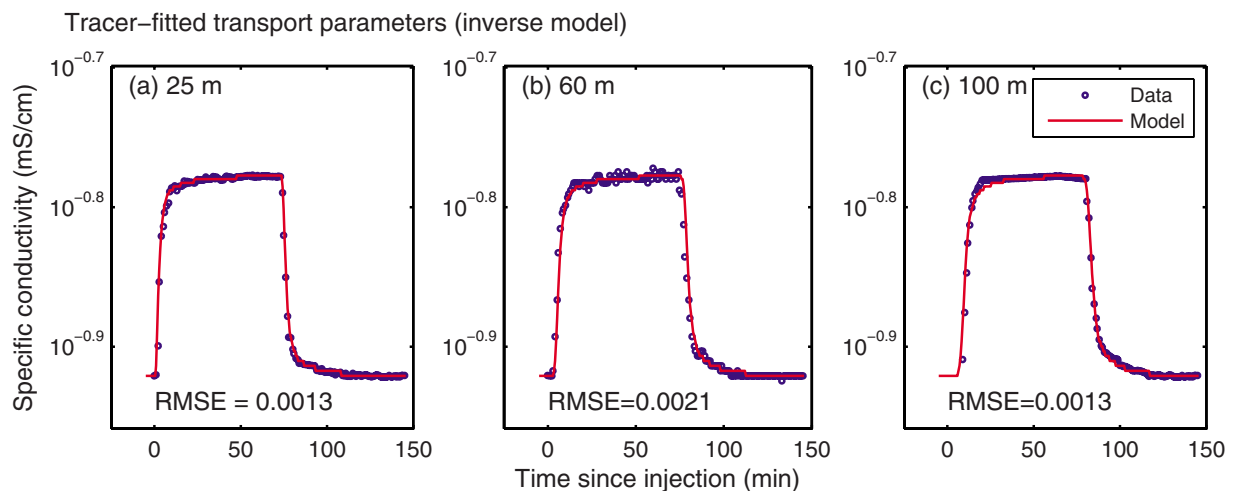


Fig. 7. Specific conductivity breakthrough curves located at (a) $x=25$ m, (b) $x=60$ m; and (c) $x=100$ m representing the upper, middle, and lower reaches, respectively. Simulated breakthrough curves were generated by fitting transport parameters to measured breakthrough curves at $x=25$ m and $x=100$ m (inverse model). The specific conductivity breakthrough curve at $x=60$ m was not used to fit transport parameters.

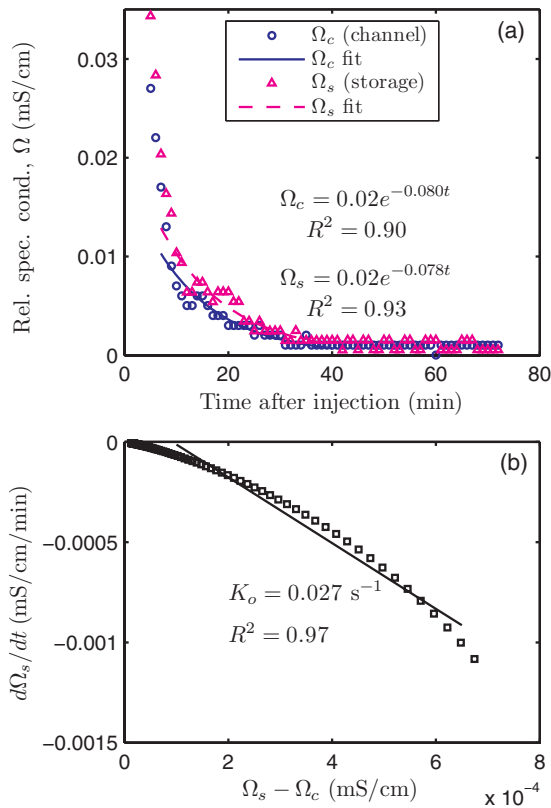


Fig. 8. Analysis of exchange between the main channel and surface storage zone located 60 m downstream. (a) Relative specific conductivity (Ω , base-line subtracted) breakthrough curves in the channel and the embayment; (b) first-order analysis of the exchange rate, K_o .

tracted) for the channel and the storage zone (Fig. 8). The exponential rate coefficient in the storage zone was smaller than that of the main channel indicating the degree of transient storage [Fig. 8(a)]. Fig. 8(b) depicts Eq. (7) from which the first-order exchange coefficient, $K_o = 0.027 \text{ s}^{-1}$, was estimated. The physically based estimate of K_o [Eq. (9)] was calculated assuming $k=0.03$, $h=0.25 \text{ m}$, $h_s=0.15 \text{ m}$, $w=1 \text{ m}$, and $U=0.50 \text{ m/s}$ resulted in $K_o=0.025 \text{ s}^{-1}$, which implied that $E=0.02 \text{ m/s}$ [Eq. (8)].

Nitrate Uptake

Measured NO_3^- concentrations taken from grab samples during the plateau period of the stream tracer injection declined exponentially along the reach (Fig. 9). Error bars indicated that there was considerable variability in NO_3^- concentrations collected at varying times and locations in each cross section over the duration of the tracer plateau. The data for the downstream tracer reach ($x=35\text{--}95 \text{ m}$) produced a value of $S_w=200 \text{ m}$ ($R^2=0.98$) according to the nutrient spiraling model [Eqs. (2) and (3)].

Both sets of transport parameters (tracer fitted and measured/scaled) were used with the OTIS-P model to fit the reaction terms λ and λ_s (Table 3). For the forward transport model (measured/scaled transport parameters), the downstream tracer reach ($x=35\text{--}95 \text{ m}$) was simulated using the lower reach transport parameters. Both the forward and inverse transport models generated greater reaction rates in the storage zone compared to the main channel ($\lambda_s > \lambda$). The COV values were consistent between transport models with larger uncertainties for λ_s . The greatest

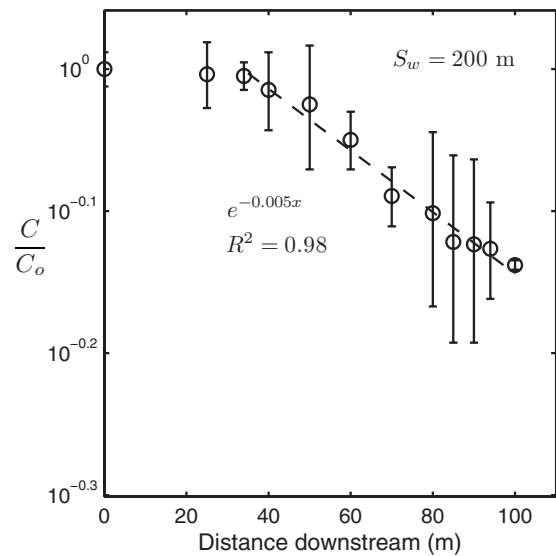


Fig. 9. Nitrate (NO_3^-) concentrations taken along the study reach during the tracer plateau. The slope of the regression line for the downstream tracer reach ($x=35\text{--}95 \text{ m}$) was used with the nutrient spiraling model [Eq. (3)] to determine the uptake length, S_w . Error bars indicate the standard deviation in replicate samples taken at various points in each cross section and at varying times during the tracer plateau.

difference between the transport models was in the percent NO_3^- uptake between the main channel and the storage zone for the upstream tracer reach. The inverse transport model gave an approximate 50/50% split while the forward transport model gave an approximate 70/30% split between uptake in the channel and the storage zone, respectively.

Both models matched the biosensor measured NO_3^- concentrations for the upstream reach [Fig. 10(a)]. However, both models slightly underestimated NO_3^- concentrations on the initial rise and overestimated NO_3^- concentrations on the falling limb of the tracer plateau for the downstream reach [Fig. 10(b)]. The measured NO_3^- concentration time series did not reach a steady plateau value, but instead slowly decreased with time during the plateau phase of

Table 3. Estimates of the kinetic parameters (λ and λ_s) and fraction of nitrate (NO_3^-) uptake between the main channel and storage zone estimates for the upstream and downstream tracer reaches; results are given for transient storage model simulations using tracer-fitted (inverse model) and measured/scaled (forward model) transport parameters; values in brackets are the coefficients of variation for the parameter estimates

Reach	λ (s^{-1})	λ_s (s^{-1})	Uptake channel (%)	Uptake storage (%)
Tracer-fitted values (inverse transport model)				
Up	2.39×10^{-4} [0.63]	7.64×10^{-4} [1.24]	54	46
Down	2.31×10^{-4} [0.31]	4.26×10^{-4} [2.68]	61	39
Measured/scaled values (forward transport model)				
Up	3.47×10^{-4} [0.42]	5.46×10^{-4} [0.33]	71	29
Down	5.46×10^{-4} [0.33]	7.38×10^{-4} [0.95]	60	40

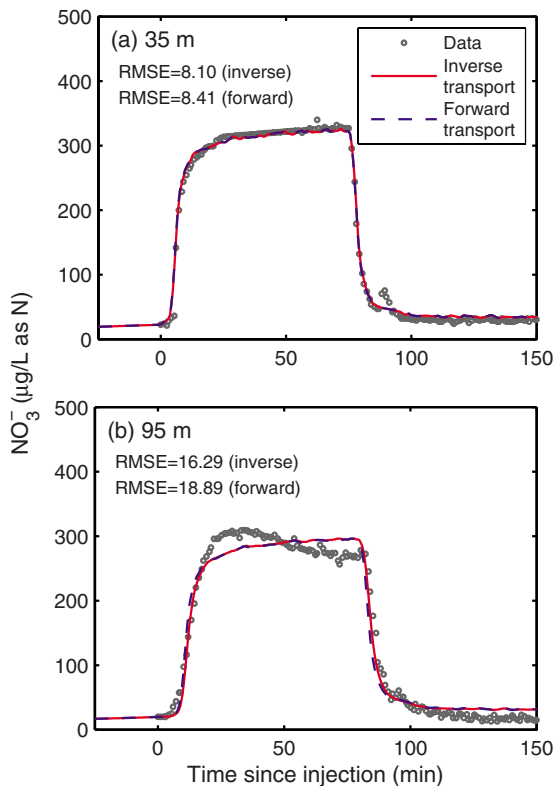


Fig. 10. Measured and modeled nitrate (NO_3^-) concentrations for the (a) upstream; (b) downstream tracer reaches

the tracer experiment suggesting time-dependent uptake kinetics. The OTIS algorithm of the transient storage model assumes that λ and λ_s are constant with time, so the simulated NO_3^- concentrations averaged the measured NO_3^- concentrations during the plateau phase of the tracer experiment [Fig. 10(b)].

The downstream reach ($x=35\text{--}95$ m) was used to assess the NO_3^- uptake rates between the nutrient spiraling and transient storage models. Biosensor-measured NO_3^- concentration curves between the upstream and downstream reaches resulted in a loss of 39 g of NO_3^- as N. The transient storage model gave a mass loss of 43 g of NO_3^- as N (10% overestimate) using tracer-fitted transport parameters and a mass loss of 31 g of NO_3^- as N (20% underestimate) using measured/scaled transport parameters. For the nutrient spiraling model, $S_w=200$ m for the downstream tracer reach. The NO_3^- tracer plateau concentration at 35 m downstream was used for C_o (350 $\mu\text{g/L}$ as N), $Q=0.205$ m^3/s , $L=60$ m, and $U=0.17$ m/s was assumed over the 60-m reach ($U=Q/A$, where $A=1.2$ m^2 for the downstream reach) and Eq. (19) resulted in a loss of 7 g of NO_3^- as N (82% underestimate).

Discussion

Reactive Transport Modeling of Elder Creek

Nutrient uptake rates were strongly dependent upon characterizing transport processes as shown by the differences in percent NO_3^- mass loss between the transient storage and nutrient spiraling models (Table 4). The nutrient uptake length of $S_w=200$ m is comparable to the results presented in the interbiome study by Mulholland et al. (2008), but it underestimated the NO_3^- mass loss by 82%. The transient storage model provided a better representation

Table 4. Comparison of the Mass of Nitrate (NO_3^-) Loss over the Downstream Tracer Reach between Measured NO_3^- Concentration and Simulated NO_3^- Breakthrough Curves, as well as the Nutrient Spiraling Model according to Eq. (19)

Area under breakthrough curve	NO_3^- loss (g as N)	Difference (%)
Measured NO_3^- biosensor data	39	
Simulated NO_3^- OTIS fitted transport	43	+10
Simulated NO_3^- measured/scaled transport	31	-20
Nutrient spiraling	7	-82

of the NO_3^- mass loss, and (in combination with NO_3^- breakthrough curves) allowed for the separation of uptake rates between the main channel and storage zone. The assumption of enhanced nutrient uptake in storage zones was not supported by the results of this study, which suggested and that uptake processes in the main channel were important. While the first-order uptake rates were greater in the storage zone than the main channel ($\lambda_s > \lambda$), the residence time in the main channel was greater than that in the storage zones ($t_c > t_s$).

Both the nutrient spiraling and transient storage models depict nutrient uptake as a first-order process. The nutrient spiraling method of determining S_w makes the assumption that steady-state concentrations exist (either under ambient conditions or during the plateau of a tracer experiment) when solving the linearized version of Eq. (3). However, replicate grab samples taken at varying times during the tracer plateau and at varying points in the cross section demonstrated a high degree of spatial and temporal variability in the NO_3^- concentrations represented by the error bars in Fig. 9. The sag in the NO_3^- plateau for the downstream breakthrough curve [Fig. 10(b)] suggested that the kinetics of NO_3^- uptake varied with time over the course of the experiment, and the transient storage model fitted steady state kinetic terms (λ and λ_s) to average the plateau region (Fig. 10). Since the transient storage model simulations did a significantly better job in matching NO_3^- mass loss values, the effect of time varying uptake kinetics was not as important as transient storage effects in quantifying nutrient uptake.

The Elder Creek study reach had very contrasting transport conditions from the upper pool, middle riffle, and lower pool over a relatively short distance (100 m), which is characteristic of many stream restoration designs. Quantifying the transport parameters of the transient storage model under such circumstances was challenging. For this study, the traditionally used conservative tracer fitting method was not able to produce a converged set of transport parameters for the middle and lower reaches individually. The large DaI value for the middle-riffle reach was a result of the fast exchange rate with the embayment surface storage zone resulting in “equilibrium mixing” as described by Wagner and Harvey (1997). Essentially, the fast exchange with surface storage zones results in the nonadvective component of solute transport being accounted for by dispersion rather than storage zone exchange. Conversely, the measured and scaled set of transport parameters produced a good fit to the measured breakthrough curves and these values were obtained by relatively simple measurements of hydraulic and channel form variables.

Measured transport parameters were chosen over scaled estimates in the forward model for the conservative solute breakthrough curves, but its not always feasible to measure all transient storage variables. For example, it was not possible to measure A_s

and α based on channel cross sections and velocity data for the upper- and lower-pool reaches where transient storage was controlled by dead zones of undefined geometry. As an alternative, the scaling relationships for A_s [Eq. (12), Harvey and Wagner 2000] and α [Eq. (13), Cheong et al. 2007] used in this study produced similar values to those fitted to the conservative tracer. Both of these scaling relationships were generated from empirical data collected under a wide range in stream conditions and each have a certain degree of uncertainty that can generate error in the estimates of transport parameters. In the case of D_x , a wide variety of scaling relationships have been developed, which are often more targeted to a narrower range of more specific stream conditions (Seo and Cheong 1998). Scaling relationships that are targeted to a narrow range in stream conditions can limit the uncertainty of scaled transport parameter estimates, so further development empirically based scaling relationships for transport parameters is warranted, especially for the A_s and α terms.

Exchange with surface storage zones was quantified reasonably well using the first-order theory as described by Valentine and Wood (1979) and Uijttewaai et al. (2001). Almost identical results of K_o were obtained using tracer data [Eq. (7), Fig. 8] and physical measurements of U and embayment geometry [Eqs. (8) and (9)] for the large embayment located at $x=60$ m downstream. This large embayment surface storage zone was assumed to control the transient storage of the middle-riffle reach characterized by high velocities, shallow water depths, and boulder obstructions [Fig. 3(d)]. The values of α [Eq. (10)] and A_s (interfacial area for the embayment) used in the forward model simulation match the measured conservative tracer breakthrough curve [Fig. 6(b)], which confirmed the assumption of the large embayment controlling the transient storage in this subreach.

Limitations of the Nutrient Spiraling Model

The nutrient spiraling model does not account for transient storage processes in quantifying nutrient uptake rates, which are important in determining the total residence time. According to the nutrient spiraling model that assumed advection only, the residence time in the downstream reach ($L/U=5.9$ min) was less than that estimated by the transient storage model ($t_c+t_s=8.2$ min) resulting in less time for uptake reactions to occur. The fact that this difference in total residence time was relatively small between the two models, and yet the transient storage model did a much better job of representing the total NO_3^- mass loss, shows how important it is to accurately characterize transport processes for quantifying nutrient uptake.

Previous studies examining intersite comparisons of nutrient uptake and stream conditions have examined the nutrient spiraling metrics of S_w , mass transfer velocity ($v_f=Uh/S_w$), and uptake flux ($U_n=UhC/S_w$) in order to account for hydraulic differences between streams (e.g., Hall et al. 2002). However, these metrics only account for U and h , which are both reach-averaged values. The role of hyporheic and surface storage zones are not accounted for, which can have dramatic effects given that D_x , A_s , and α vary over several orders of magnitude among the stream tracer experiments compiled by Ensign and Doyle (2006). Another approach used in previous studies has been to examine both nutrient spiraling metrics and transport parameters of the transient storage model together (e.g., Hall et al. 2002; Ensign and Doyle 2005; Lautz and Siegel 2007; Roberts et al. 2007). However, since the nutrient spiraling metrics are not independent of the stream's hydrology (Runkel 2007) and can produce a large error in interpret-

ing the mass loss in a reach, it raises the question: to what extent do the nutrient spiraling metrics actually represent nutrient uptake? The key to this question is to recognize that quantifying nutrient uptake rates requires use of a reactive transport model. In the case of the nutrient spiraling model, hydraulics and biogeochemistry are lumped in the nutrient uptake metrics. The advantage of the transient storage model is that its uptake metrics, λ and λ_s , are independent of the stream's hydrology and thus more accurately represent the biological and biogeochemical processes controlling nutrient uptake.

Importance of Measured and Scaled Transport Parameters

Inverse modeling of conservative tracer data provides accurate estimations of transport parameters for a given set of stream conditions, but they can be difficult to apply to varying flow or geomorphic conditions of the same or a different stream. Additionally, stream tracer experiments are sensitive to the range in spatial and temporal scales of the transport processes involved, especially in the case of complex stream conditions where transport can be controlled by both hyporheic exchange and surface storage zones that operate on very different spatial and temporal scales (Harvey and Wagner 2000). Quantifying transport parameters using measurements and scaling relationships is advantageous to fitting conservative tracer data for restoration purposes because the estimates can be more readily applied over a wide range of hydraulic and channel form design scenarios. As mentioned previously, the issue with using scaling relationships is the uncertainty in transport parameter estimates. Therefore, future work on the development and verification of scaling relationships for varying stream conditions with physical measurements of transport processes is needed.

Some recent studies have treated transient storage modeling using more than one storage zone to represent multiple transport processes operating on different time scales (Choi et al. 2000; Gooseff et al. 2004), as well as to potentially separate surface and hyporheic storage zones (Harvey et al. 2005; Briggs et al. 2009). While this approach has appeal in representing physically distinct transient storage processes, each additional storage zone adds an additional two terms (A_s and α) that must be parameterized. The addition of transport parameters beyond a single storage zone can exceed the capability of tracer fitting approaches in uniquely identifying transport parameters (Harvey and Wagner 2000). The methods for quantifying transport processes presented in this study could be used with a stream tracer experiment to limit the number of fitted parameters in these multistorage zone modeling approaches. The first-order exchange theory presented in Eqs. (7)–(10) can be used to estimate exchange parameters for surface storage zones. For hyporheic exchange there are no simple techniques for quantifying A_s and α , but there has been some progress with respect to relating hyporheic exchange to stream conditions (Wörman et al. 2002; O'Connor and Harvey 2008) that could be used to develop such techniques for quantifying hyporheic-based A_s and α values.

Predictive Models of Nutrient Uptake for Stream Restoration

Predicting nutrient uptake rates is challenging and yet to advance stream restoration for improving water quality, engineers need to

Table 5. Proposed Steps for Quantifying Nutrient Uptake, Transient Storage, and the Development of Predictive Reactive Transport Models for Stream Restoration

Task	Considerations/methods	Notes	Resources
Stream tracer experiment design	Nutrient or isotope addition	Bulk uptake or specific reaction pathway Concentration effects	Böhlke et al. (2004), Payn et al. (2005) Dodds et al. (2002)
	Selection of reaches	Reaches should reflect similar geomorphology and transport conditions (pools and riffles)	
	Solute injection rate and duration	Discharge, reach length, and sensitivity of tracer measurement	Harvey and Wagner (2000)
	Breakthrough curves or steady-state assumption	Total mass loss from breakthrough curves only	
Quantify transport parameters	Conservative tracer	“Window of detection” factors Results only applicable to stream conditions during tracer	Harvey and Wagner (2000)
	Physical measurements	ADV, ADCP, 2D, and 3D hydraulic models	Eqs. (6), (8), and (10)
	Scaling relationships	Verify ranges in channel and hydraulic variables of study reach with those in scaling expression derivation	Seo and Cheong (1998); Harvey and Wagner (2000); Cheong et al. (2007) Eqs. (11)–(13)
<i>(Physical measurements and scaling relationships preferable for stream restoration, applicable over varying channel form and hydraulic conditions)</i>			
Quantify nutrient uptake rates	Breakthrough curves	Nonlinear regression techniques (OTIS-P) Main channel/storage zone uptake	Runkel (1998, 2007)
	Steady-state assumption	Need to address the effects of transient storage processes	Runkel (2007)
<i>(Breakthrough curves partition uptake between main channel and storage zones, can address debate over role of storage zones on uptake)</i>			
Synthesis of nutrient uptake	Previous studies using nutrient spiraling model	Is there ancillary data available to assess the effects of transient storage processes?	
	Assemble uptake rates with controlling variables	Transport processes	This study
		Algal communities	Baker et al. (2009)
		Bacterial communities	Lefebvre et al. (2005)
		Carbon quantity and quality	Holmes et al. (1996)
Temporal effects (e.g., seasonal)	von Schiller et al. (2008)		
Develop predictive expressions for nutrient uptake	Multivariate regression Dimensional analysis (scaling) Artificial neural networks	Lautz and Siegel (2007) O’Connor et al. (2006) Aitkenhead et al. (2007)	
<i>(Substantial work in needed in developing predictive expressions for nutrient uptake with relation to hydraulics and channel form)</i>			

be able to relate uptake rates to channel and hydraulic conditions (design variables). Table 5 summarizes the process of obtaining reach-scale nutrient uptake rates, quantifying transport processes, and methods for developing empirically based predictive relationships for nutrient uptake that are need for the evaluation of stream restoration design scenarios. The first step in this process is to make sure that our methods for quantifying nutrient uptake rates are accurate. The results from this study suggest that it is vital to incorporate dispersion and transient storage processes for inferring nutrient uptake rates using stream tracers. It is helpful to have measured nutrient breakthrough curves as it allows for the quantification of the mass loss, assessing the temporal variability in reaction kinetics, and partitioning nutrient uptake between the main channel and the storage zones. Additionally, physical measurements and the continued development of scaling relationships of transport parameters are needed in order to improve reactive transport modeling efforts, especially in complex systems containing multiple transient storage processes occurring over a wide range in temporal and spatial scales.

Conclusions

The transient storage model is preferable to nutrient spiraling for quantifying nutrient uptake because transport processes and biogeochemical kinetics are more accurately represented. Transient storage greatly affects nutrient uptake by controlling the residence time and is significant in hyporheic and surface storage zones, as well as in the main channel (e.g., dispersion). Determining the role of nutrient uptake between the main channel and storage zones is crucial for stream restoration designs, which requires quantifying transient storage processes in complex geomorphic settings. Limitations associated with fitting transport parameters to conservative tracer data can be overcome with the use of physical measurement and scaling techniques, which can be applied to a broader range of stream conditions. Ultimately, empirically based relationships quantifying nutrient uptake in relation to hydraulic and geomorphic conditions are needed for stream restoration because physical variables are what engineers can base restoration designs on. The development of such predictive reactive transport models requires that future studies give equal emphasis to the quantification of both nutrient uptake and transport processes.

Acknowledgments

The manuscript was prepared while B.L. O'Connor held a National Research Council (NRC) Research Associateship Award at USGS in Reston, Virginia. OTIS modeling assistance was provided by Lauren McPhillips (USGS). Funding was provided by the National Center for Earth-surface Dynamics (NCED), a Science and Technology Center funded by the Office of Integrative Activities of the National Science Foundation (NSF) (under Agreement No. EAR-0120914), as well as the National Water Quality Assessment (NAWQA) and National Research programs of the USGS. Funding for J.W. Harvey was also provided by NSF (under Agreement No. EAR-0814990). Earlier versions of the manuscript were improved upon thanks to comments from colleague reviewers Cailin Huyck Orr and Harry Jenter, as well as journal reviewers Peter Wilcock and an anonymous reviewer. Any

use of trade, firm, or product names is for descriptive purposes only and does not imply endorsement by the U.S. Government.

Notation

The following symbols are used in this paper:

- A = channel cross section area [L^2];
- A_s = storage zone cross section area [L^2];
- B = stream width [L];
- C = concentration [M/L^3];
- C_o = concentration at the start of a reach [M/L^3];
- C_s = concentration in the storage zone [M/L^3];
- D_x = longitudinal dispersion coefficient [L^2/T];
- D_y = transverse mixing coefficient [L^2/T];
- DaI = Damkohler number for stream tracer experiment;
- E = entrainment velocity [L/T];
- F_{med} = fraction of median travel time due to transient storage;
- f = Darcy-Weisbach friction coefficient;
- h = water depth in the main channel [L];
- h_s = water depth in surface storage zone [L];
- K_o = exchange coefficient with surface storage zone [T^{-1}];
- k = dimensionless exchange coefficient;
- L = reach length [L];
- l = length of surface storage zone [L];
- M = solute mass integrated under tracer curve [M];
- M_c = integrated mass for uptake in the main channel only [M];
- M_r = integrated mass for reactive transport model [M];
- M_s = integrated mass for uptake in the storage zone only [M];
- M_t = integrated mass for conservative transport model [M];
- Q = discharge [L^3/T];
- S_w = nutrient spiraling uptake length [L];
- Si = sinuosity ratio;
- t = time [T];
- t_c = mean residence time in main channel [T];
- t_s = mean residence time in storage zone [T];
- U = cross-sectional averaged velocity [L/T];
- U_n = nutrient uptake flux [$M/L^2/T$];
- u = streamwise velocity component [L/T];
- u_* = shear stress velocity [L/T];
- \bar{u} = depth-averaged streamwise velocity [L/T];
- v = transverse velocity [L/T];
- v_f = nutrient uptake velocity [L/T];
- w = width of surface storage zone [L];
- x = stream wise coordinate, distance downstream [L];
- y = transverse coordinate, distance from right bank [L];
- α = exchange rate with storage zone [T^{-1}];
- γ = correction factor in Eqs. (17) and (18);
- $\Delta M_{channel}$ = mass loss for model assuming uptake in the main channel only [M];
- $\Delta M_{spiraling}$ = mass loss for nutrient spiraling model [M];
- $\Delta M_{storage}$ = mass loss for model assuming uptake in the storage zone only [M];

- ΔM_{total} = mass loss for reactive transport model [M];
 λ = uptake coefficient in the channel [T^{-1}];
 λ_s = uptake coefficient in storage zone [T^{-1}];
 Ω_c = relative specific conductivity in main channel [$Q^2 T^3 / ML^3$]; and
 Ω_s = relative specific conductivity in surface storage zone [$Q^2 T^3 / ML^3$].

References

- Aitkenhead, M. J., Aitkenhead-Peterson, J. A., McDowell, W. H., Smart, R. P., and Cresser, M. S. (2007). "Modelling DOC export from watersheds in Scotland using neural networks." *Comput. Geosci.*, 33, 423–436.
- Alexander, R. B., et al. (2009). "Dynamic modeling of nitrogen losses in river networks unravels the coupled effects of hydrological and biogeochemical processes." *Biogeochemistry*, 93(1–2), 91–116.
- American Public Health Association (APHA). (1998). *Standard methods for examination of water and wastewater*, 20th Ed., Washington, D.C.
- Baker, M. A., de Guzman, G., and Ostermiller, J. D. (2009). "Differences in nitrate uptake among benthic algal assemblages in a mountain stream." *J. North Am. Benthol. Soc.*, 28(1), 24–33.
- Bernhardt, E. S., et al. (2005). "Synthesizing U.S. river restoration efforts." *Science*, 308(5722), 636–637.
- Bernhardt, E. S., Likens, G. E., Guso, D. C., and Driscoll, C. T. (2003). "In-stream uptake dampens effects of major forest disturbance on watershed nitrogen export." *Proc. Natl. Acad. Sci. U.S.A.*, 100(18), 10304–10308.
- Böhlke, J. K., Harvey, J. W., and Voytek, M. A. (2004). "Reach-scale isotope tracer experiment to quantify denitrification and related processes in a nitrate-rich stream, midcontinent United States." *Limnol. Oceanogr.*, 49(3), 821–838.
- Briggs, M. A., Gooseff, M. N., Arp, C. D., and Baker, M. A. (2009). "A method for estimating surface transient storage parameters for streams with concurrent hyporheic storage." *Water Resour. Res.*, 45, W00D27.
- Bukaveckas, P. A. (2007). "Effects of channel restoration on water velocity, transient storage, and nutrient uptake in a channelized stream." *Environ. Sci. Technol.*, 41(5), 1570–1576.
- Carr, M. L., and Rehmann, C. R. (2007). "Measuring the dispersion coefficient with acoustic Doppler current profilers." *J. Hydraul. Eng.*, 133(8), 977–982.
- Cheong, T. S., Younis, B. A., and Seo, I. W. (2007). "Estimation of key parameters in model for solute transport in rivers and streams." *Water Resour. Manage.*, 21, 1165–1186.
- Choi, J., Harvey, J. W., and Conklin, M. H. (2000). "Characterizing multiple timescales of stream and storage zone interaction that affect solute fate and transport in streams." *Water Resour. Res.*, 36(6), 1511–1518.
- Craig, L. S., et al. (2008). "Stream restoration strategies for reducing river nitrogen loads." *Front. Ecol. Environ.*, 6(10), 529–538.
- Dodds, W. K., et al. (2002). "N uptake as a function of concentration in streams." *J. North Am. Benthol. Soc.*, 21(2), 206–220.
- Ensign, S. H., and Doyle, M. W. (2005). "In-channel transient storage and associated nutrient retention: Evidence from experimental manipulations." *Limnol. Oceanogr.*, 50(6), 1740–1751.
- Ensign, S. H., and Doyle, M. W. (2006). "Nutrient spiraling in streams and river networks." *J. Geophys. Res.*, 111, G04009.
- Fischer, H. B. (1967). "The mechanics of dispersion in natural streams." *J. Hydr. Div.*, 93(6), 187–216.
- Fischer, H. B. (1975). "Discussion of 'Simple method for predicting dispersion in streams' by R.S. McQuivey and T.N. Keefer." *J. Envir. Engrg. Div.*, 101(3), 453–455.
- Gooseff, M. N., LaNier, J., Haggerty, R., and Kokkeler, K. (2005). "Determining in-channel (dead zone) transient storage by comparing solute transport in a bedrock channel-alluvial channel sequence, Oregon." *Water Resour. Res.*, 41, W06014.
- Gooseff, M. N., McKnight, D. M., Runkel, R. L., and Duff, J. H. (2004). "Denitrification and hydrologic transient storage in a glacial meltwater stream, McMurdo Dry Valleys, Antarctica." *Limnol. Oceanogr.*, 49(5), 1884–1895.
- Groffman, P. M., et al. (2006). "Methods for measuring denitrification: Diverse approaches to a difficult problem." *Ecol. Appl.*, 16(6), 2091–2122.
- Groffman, P. M., Dorsey, A. M., and Mayer, P. M. (2005). "N processing within geomorphic structures in urban streams." *J. North Am. Benthol. Soc.*, 24(3), 613–625.
- Hall, R. O., Jr., Bernhardt, E. S., and Likens, G. E. (2002). "Relating nutrient uptake with transient storage in forested mountain streams." *Limnol. Oceanogr.*, 47(1), 255–265.
- Harvey, J. W., Saiers, J. E., and Newlin, J. T. (2005). "Solute transport and storage mechanisms in wetlands of the Everglades, south Florida." *Water Resour. Res.*, 41, W05009.
- Harvey, J. W., and Wagner, B. J. (2000). "Quantifying hydrologic interactions between streams and their subsurface hyporheic zones." *Streams and ground waters*, J. B. Jones and P. J. Mulholland, eds., Academic, San Diego, 3–44.
- Holmes, R. M., Jones, J. B., Fisher, S. G., and Grimm, N. B. (1996). "Denitrification in a nitrogen-limited stream ecosystem." *Biogeochemistry*, 33, 125–146.
- Kasahara, T., and Hill, A. R. (2006). "Effects of riffle-step restoration on hyporheic zone chemistry in N-rich lowland streams." *Can. J. Fish. Aquat. Sci.*, 63, 120–133.
- Kemp, M. J., and Dodds, W. K. (2002). "The influence of ammonium, nitrate, and dissolved oxygen concentrations on uptake, nitrification, and denitrification rates associated with prairie stream substrata." *Limnol. Oceanogr.*, 47(5), 1380–1393.
- Kim, B. K. A., Jackman, A. P., and Triska, F. J. (1992). "Modeling biotic uptake by periphyton and transient hyporheic storage of nitrate in a natural stream." *Water Resour. Res.*, 28(10), 2743–2752.
- Lautz, L. K., and Siegel, D. I. (2007). "The effect of transient storage on nitrate uptake lengths in streams: An inter-site comparison." *Hydrolog. Process.*, 21(26), 3533–3548.
- Lefebvre, S., Marmonier, P., Pinay, G., Bour, O., Aquilina, L., and Baudry, J. (2005). "Nutrient dynamics in interstitial habitats of low-order rural streams with different bedrock geology." *Archiv Hydrobiol.*, 164(2), 169–191.
- Mulholland, P. J., et al. (2008). "Stream denitrification across biomes and its response to anthropogenic nitrate loading." *Nature*, 452(13), 202–205.
- Newbold, J. D., Elwood, J. W., O'Neill, R. V., and Van Winkle, W. (1981). "Measuring nutrient spiralling in streams." *Can. J. Fish. Aquat. Sci.*, 38, 860–863.
- O'Connor, B. L., and Harvey, J. W. (2008). "Scaling hyporheic exchange and its influence on biogeochemical reactions in aquatic ecosystems." *Water Resour. Res.*, 44, W12423.
- O'Connor, B. L., Hondzo, M., Dobraca, D., LaPara, T. M., Finlay, J. C., and Brezonik, P. L. (2006). "Quantity-activity relationship of denitrifying bacteria and environmental scaling in streams of a forested watershed." *J. Geophys. Res.*, 111, G04014.
- Opdyke, M. R., David, M. B., and Rhoads, B. L. (2006). "Influence of geomorphological variability in channel characteristics on sediment denitrification in agricultural streams." *J. Environ. Qual.*, 35, 2103–2112.
- Orr, C. H., Clark, J. J., Wilcock, P. R., Finlay, J. C., and Doyle, M. W. (2009). "Comparison of morphological and biological control of exchange with transient storage zones in a field-scale flume." *J. Geophys. Res.*, 114, G02019.
- Payn, R. A., Webster, J. R., Mulholland, P. J., Valett, H. M., and Dodds, W. K. (2005). "Estimation of stream nutrient uptake from nutrient addition experiments." *Limnol. Oceanogr. Methods*, 3, 174–182.
- Richardson, W. B., Strauss, E. A., Bartsch, L. A., Monroe, E. M., Cavanaugh, J. C., Vingum, L., and Soballe, D. M. (2004). "Denitrification in the Upper Mississippi River: Rates, controls, and contribution to nitrate flux." *Can. J. Fish. Aquat. Sci.*, 61, 1102–1112.

- Roberts, B. J., Mulholland, P. J., and Houser, J. N. (2007). "Effects of upland disturbance and instream restoration on hydrodynamics and ammonium uptake in headwater streams." *J. North Am. Benthol. Soc.*, 26(1), 38–53.
- Runkel, R. L. (1998). "One-dimensional transport with inflow and storage (OTIS)." *Water Resour. Invest. Rep. No. 98-4018*, USGS, Denver, Colo.
- Runkel, R. L. (2002). "A new metric for determining the importance of transient storage." *J. North Am. Benthol. Soc.*, 21(4), 529–543.
- Runkel, R. L. (2007). "Toward a transport-based analysis of nutrient spiraling and uptake in streams." *Limnol. Oceanogr. Methods*, 5, 50–62.
- Rutherford, J. C. (1994). *River mixing*, Wiley, West Sussex, U.K.
- Seo, I. W., and Cheong, T. S. (1998). "Predicting longitudinal dispersion coefficient in natural streams." *J. Hydraul. Eng.*, 124(1), 25–32.
- Shields, F. D., Jr., Copeland, R. R., Klingeman, P. C., Doyle, M. W., and Simon, A. (2003). "Design for stream restoration." *J. Hydraul. Eng.*, 129(8), 575–584.
- Smith, L. K., Voytek, M. A., Böhlke, J. K., and Harvey, J. W. (2006). "Denitrification in nitrate-rich streams: Application of N₂:Ar and ¹⁵N-tracer methods in intact cores." *Ecol. Appl.*, 16(6), 2191–2207.
- Thackston, E. L., and Schnelle, K. B., Jr. (1970). "Predicting effects of dead zones on stream mixing." *J. Sanit. Engrg. Div.*, 96(SA2), 319–331.
- Triska, F. J., Kennedy, V. C., Avanzino, R. J., Zellweger, G. W., and Bencala, K. E. (1989). "Retention and transport of nutrients in a third-order stream: Channel processes." *Ecology*, 70(6), 1877–1892.
- Uijttewaal, W. S. J., Lehmann, D., and van Mazijk, A. (2001). "Exchange processes between a river and its groyne fields: Model experiments." *J. Hydraul. Eng.*, 127(11), 928–936.
- Valentine, E. M., and Wood, I. R. (1979). "Experiments in longitudinal dispersion with dead zones." *J. Hydr. Div.*, 105(8), 999–1016.
- von Schiller, D., et al. (2008). "Inter-annual, annual, and seasonal variation of P and N retention in a perennial and an intermittent stream." *Ecosystems*, 11(5), 670–687.
- Wagner, B. J., and Harvey, J. W. (1997). "Experimental design for estimating parameters of rate-limited mass transfer: Analysis of stream tracer studies." *Water Resour. Res.*, 33(7), 1731–1741.
- Warnaars, T. A., Hondzo, M., and Power, M. E. (2007). "Abiotic controls on periphyton accrual and metabolism in streams: Scaling by dimensionless numbers." *Water Resour. Res.*, 43, W08425.
- Weitbrecht, V., Socolofsky, S. A., and Jirka, G. H. (2008). "Experiments on mass exchange between groin fields and main stream in rivers." *J. Hydraul. Eng.*, 134(2), 173–183.
- Wörman, A., Packman, A. I., Johansson, H., and Jonsson, K. (2002). "Effect of flow-induced exchange in hyporheic zones on longitudinal transport of solutes in streams and rivers." *Water Resour. Res.*, 38(1), 1001.